ANALYSIS OF INFLUENCE OF GEOMETRIC AND VELOCITY FEATURES ON THE FAR-FIELD NOISE OF COPLANAR JETS

Fábio Garcia Temístocles Ferreira, fabiogtf@bol.com.br
Odenir de Almeida, odenir@mecanica.ufu.br
Universidade Federal de Uberlândia, Av. João Naves de Ávila, 2121, 5P Building, Uberlândia - Brazil.

Abstract. *The noise generated by an airplane in operation has been focus of attention of the new researches. Since the jet exhaust is one of the most important noise sources, this work's proposal is to analyze dual stream coaxial jets. For this, it was employed an average approach (RANS) with the cubic k-ε turbulence model in order to obtain the aerodynamic field. So, the jet flow must be well resolved and understood especially with respect to the geometry and operation conditions in order to obtain good predictions of the global far-field noise. The operation conditions like the velocity ratio (VR), and geometry aspect (given by the area ratio or AR) of the nozzle are highlighted by literature. From these considerations, this work proposes to study the influence of the area ratio (ratio between the secondary and primary exhaust nozzle area) and the velocity ratio (analogous for velocity) of a coplanar jet on its fluid dynamics behavior and then on the aeroacoustics results. For this, bidimensional and threedimensional simulations have been carried out with different configurations, in order to compare these results with the experimental data available. The mean flow of the bidimensional simulations is compared with the experimental data, and the three-dimensional results are used to seed the far-field noise calculation model called "waveprop" based on the volumetric integral solution of Curlie's equation. The methodology applied is implemented in the commercial code CFD++/CAA++ distributed by Metacomp Inc, which is being used in the EMBRAER/FAPESP "Aeronave Silenciosa" project.*
The results of SPL noise are substantially below the experimental data, showing some weakness or limitations in terms of the methodology applied. However, the main proposal of this work is to provide good averaged solutions for the aerodynamics. Further steps will be taken in order to enhance the far-field noise spectra.

Keywords*: Jet flow, Aeroacoustics, far-field noise, noise source, area ratio, velocity ratio.*

1. INTRODUCTION

Some important developments have been made in order to help the jet engine designers who are increasingly looking for novel methodologies that can predict the noise for the jet flows. These flows have some interesting features, and the good comprehension of the phenomena has fundamental importance on modeling the problem of jet noise. With this aim, the so called Computational Fluid Dynamics (CFD) methods associated with the modern approach called Computational Aeroacoustics (CAA) methods are evocated.

Firstly, a good solution of the fluid dynamic flow must be reached, since it is understood that the phenomena of sound generation and propagation are consequence of the interactions of shear on the fluid motion.

A popular modeling is the Reynolds-Averaged Navier-Stokes equations (RANS) and this method has the adequate characteristics to be applied on this work, since it has an industrial point of view. This method is based on the information of the averaged fluid properties which leads to a relatively less expensive calculation.

Moreover, some important decisions have to be made with respect to the turbulence model to be applied and also the methodology to evaluate the noise field through the Computational Aeroacoustics (CAA) methods, and finally to calculate the far-field noise through a noise propagation methodology.

Both, the fluid dynamic field and the noise field must be well modeled, so the whole phenomena will be took in consideration on the final result. An example is the work of Birch *et. al.* (2003), they pointed the importance to use the correct turbulence model to the type of flow on modeling a coaxial jet flow with chevrons.

After the calculation of the averaged field, the most relevant information is used to evaluate the far-field noise calculation with a model to perform only calculation and propagation of the noise. The method applied in this work is based on the volumetric integral solution, proposed by Curlie in 1970 of the Lighthill equation, of the region where the shear layers (the inner shear layer and the outer one) contributes for the generation of the noise in the exhaust jet. This method will be briefly described in section 2.2.

The analysis of the velocity ratio (VR) and area ratio (AR) is carried out using the geometry of the CoJeN (Computation of Coaxial Jet Noise) project. The experimental data and the simulation parameters are suggested by Almeida (2009). On the other hand, the quest of the influence of the area ratio is supported by the data of the JEAN (Jet Exhaust Aerodynamics and Noise) EU project, which applies a different geometry of coplanar nozzle.

Finally, the far-field Sound Pressure Level (SPL) are computed numerically and compared with the respective database of the two different sets of experimental data available. All the experimental data have been collected in collaboration with ISVR (Institute of Sound and Vibration Research) UK.

2. AERODYNAMICS AND NOISE EVALUATION

2.1. Description of the Problem

The problem simulated consists of a two stream coplanar nozzle exhaust of aeronautic engine. The presence of the second stream creates two mixing layers and shear layers which leads to a less steep gradient of the velocity profile in a global way. So in this type of flow one can find different regions as pointed by several authors like Almeida (2009) and Tam and Pastouchenko (2006). The main stream generates the potential core and the secondary one, one analogous structure in the initial region, which precedes an interaction region, and that is followed by a mixed flow region.

Two nozzle geometries are considered in this work. The Figure 1 shows the geometry of the nozzle from the CoJeN project with area ratio (secondary section area over the primary one) of AR = 3. Figure 2 shows the second type of coplanar nozzle used in this work from the JEAN project of noise evaluation, with same area ratio.

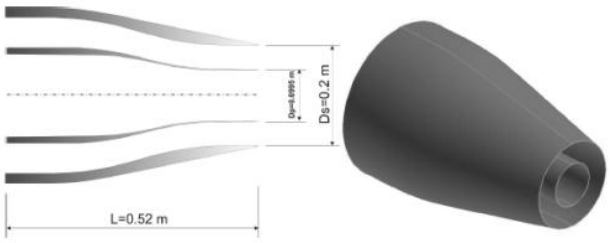

Figure 1. Geometry of the nozzle utilized on the simulations according to the COJEAN project. Adapted from Almeida (2009).

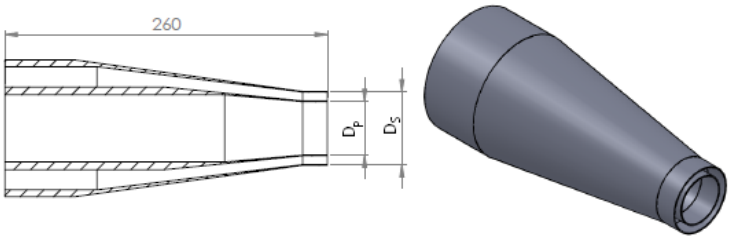

Figure 2. Geometry utilized on the simulations according to the JEAN project.

The following tables characterize the matrix of simulations carried out with both geometries. In this work, simulations were performed for the CoJeN geometry with area ratio AR=3.0 and five different values for velocity ratio VR (secondary stream speed over the primary one) as presented within Table 1. Therefore, the primary stream velocity remains constant at the value of 217.2 m/s whilst the secondary velocity varies.

On the other hand, for the JEAN geometry (Fig. 2), the simulations contemplate two values of area ratio and three values of velocity ratio varying both the secondary and the primary velocities. This is showed on the Table 2.

Table 1. Parameters of the simulations proposed for the coplanar coaxial nozzle of COJEAN geometry.

Case	VR	Vp [m/s]	Vs [m/s]	Pp [Pa]	Tp [K]	Ps [Pa]	Ts [K]
1	1.0	217.2	217.200	129790.569	311.870	129432.400	311.630
2	0.9	217.2	195.480	129790.569	311.870	123063.135	307.170
3	0.8	217.2	173.760	129790.569	311.870	117556.954	303.180
4	0.7	217.2	152.040	129790.569	311.870	112846.711	299.650
5	0.6	217.2	130.320	129790.569	311.870	108874.899	296.600

The experimental procedures of CoJeN project uses the ambient values of P = 98937.7 Pa and T = 288.15 K. Now for the JEAN project each experimental procedure assumes slightly different ambient values of temperature and pressure. The indices used here have the following meaning: *"p"* refers to the primary stream; *"s"* refers to the secondary stream; *"o"* used herewith *"p"* and *"s"* means the stagnation value and the index "∞" indicates that the value that accompanies is an ambient value.

Table 2. Parameters of simulations for the coplanar coaxial nozzle of JEAN project.

Case	AR	VR	V_p [m/s]	P_{op} [Pa]	T_{op} [K]	V_s [m/s]	P_{os} [Pa]	T_{os} [K]	P_∞ [Pa]	T_∞ [K]
1	2.0	1.0	167.0	122288.03	279.6	165.0	121468.17	279.7	102400.0	275.45
2		0.79	208.7	136020.20	279.0	167.5	122288.03	279.2	102400.0	275.56
3		0.63	209.2	136020.20	280.0	131.1	114334.92	280.4	102400.0	275.56
4	4.0	1.0	166.7	121332.65	283.9	167.9	121332.65	283.5	101600.0	279.56
5		0.79	168.3	121332.65	284.4	134.1	113441.68	284.0	101600.0	279.16
6		0.63	211.6	134957.54	283.6	134.2	113441.68	283.5	101600.0	279.76

It is possible to observe that in the first set of simulations, Table 1, the velocity gradient in the inner shear layer must be increasing since the secondary velocity get smaller, while in the outer shear layer, the shear stress is decreasing with the secondary velocity. For the CoJeN coplanar geometry this is particularly easier to assess since these simulations are made with one constant velocity for the primary stream. The relationship pointed out is not maintained on the simulations with the JEAN geometry, since the simulation values are dictated by the experimental input data and not necessarily have a baseline value kept constant along all the simulations.

Finally, a more detailed simulation is performed in order to evaluate the noise spectrum from the coplanar CoJeN geometry. This simulation had to be three-dimensional (3D) in order to assess a further volumetric integration of the averaged field to evaluate the noise sources and to proceed with the noise propagation to the far-field. Details about the noise modeling will be given in the section 2.2.

A final word is to affirm that all the simulations carried out in this work had considered approximately unheated jets, i.e. the jet flow temperature is imposed approximately the ambient value.

2.2. Computational Domain and Boundary Conditions

The size of the computational domain for all simulations is based on the previous work of Almeida (2009). The 2D computational domain discretization consisted of block structured meshes with a total of 200976 elements for the coplanar CoJeN configuration. The mesh points were concentrated to the shear layer region, and a steep jump is avoided during the blocks transitions.

For the three-dimensional simulation a prismatic domain was employed with a domain 14Ds x 14Ds x 41Ds meshed with 3926320 elements. This number is comparable to the mesh on the work of Silva et. al. (2009).

On the JEAN nozzle-configuration simulations a similar two-dimensional mesh was used. This mesh had approximately 200466 elements on a domain of 10 D_s x 44 D_s for the area ratio 2.0, and 219846 elements on the domain 10 D_s x 44 D_s for AR = 4.0.

Both domain and mesh size were built as in the Almeida's work (2009) who carried out a mesh convergence test in order to obtain a enough refinement specially on the initial region of the domain, being in agreement with the literature findings with respect to the domain size and the to the required distance to the development of the flow.

All the simulations used the boundary conditions imposed as stagnation pressure and stagnation temperature on the primary and secondary inlet. For the upstream, upper and outflow/inflow conditions, the temperature and pressure ambient were set taking into account the velocity from inside domain which allows incoming and leaving fluid. And lastly, the geometric symmetry axis (except for the three-dimensional simulation) was treated as axisymmetric flow boundary condition. The domain size and boundary conditions are generically shown in Figure 3.

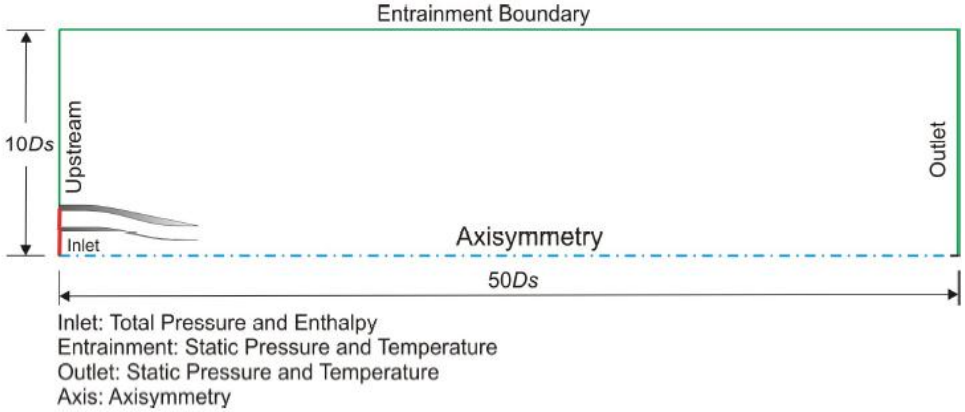

Figure 3. Domain size and boundary conditions for a coplanar coaxial nozzle.

In the three-dimensional case the same criteria was applied to the boundary conditions except the axisymmetric one. For all simulations, adjacent to the walls the Y+ value is approximately 30, so a wall function is employed to resolve the flow in this region.

2.2. Numerical Methodology

The flow field is proposed to be calculated with a Reynolds Averaged Navier-Stokes (RANS) to deal with compressible and turbulent flows by employing cubic k-ε turbulence model. The formulation for x-direction is presented below:

$$\rho\left[\frac{\partial}{\partial x}\left(\overline{u}^2\right)+\frac{\partial}{\partial y}\left(\overline{uv}\right)+\frac{\partial}{\partial z}\left(\overline{uw}\right)\right]= \\ -\frac{\partial \overline{p}}{\partial x}+\left[\frac{\partial}{\partial x}\left(\mu\frac{\partial \overline{u}}{\partial x}-\rho\overline{u'^2}\right)+\frac{\partial}{\partial y}\left(\mu\frac{\partial \overline{u}}{\partial y}-\rho\overline{u'v'}\right)+\frac{\partial}{\partial z}\left(\mu\frac{\partial \overline{u}}{\partial z}-\rho\overline{u'w'}\right)\right] \tag{1}$$

This work employs a non-linear *k-ε* turbulence model in order to obtain the turbulence variable. Details about this formulation are pointed out by Silva et. al. (2009).

After obtaining the aerodynamic field with the turbulent characteristics, an analytical tool for sound propagation was considered. The sound generation and propagation of waves is performed by reconstruction of the velocity fluctuation from the statistics (averaged field) contained within the given turbulent solution. A similar work was carried out by Silva et. al. (2007) using the tools of the commercial software – CFD++/CAA++. This procedure is based on the Lighthill's Acoustic Analogy as follows:

$$\frac{\partial^2\rho'}{\partial t^2}-c_o^2\frac{\partial^2\rho'}{\partial x_i^2}=\frac{\partial^2 T_{ij}}{\partial x_i x_j} \tag{2}$$

where T_{ij} is Lighthill's Tensor with the three terms of sound generation:

$$T_{ij}=\rho u_i u_j-\tau_{ij}+\left(p-c_\infty^2\rho\right)\delta_{ij} \tag{3}$$

The right-hand side is assumed to be known and independent of the left-hand side, which represents a wave propagator operator. Curle proposed a solution for this equation, as seen on Larsson (2002).

$$p'\left(x_i,t\right)=\frac{1}{4\pi}\iiint\left[\frac{l_i l_j}{c_\infty^2 r}\frac{\partial^2 T_{ij}}{\partial t^2}+\frac{3l_i l_j-\delta_{ij}}{c_\infty r^2}\frac{\partial T_{ij}}{\partial t}+\frac{3l_i l_j-\delta_{ij}}{r^3}T_{ij}\right]dV+ \\ \frac{1}{4\pi}\iint l_i n_j\left[\frac{i}{c_\infty^2 r}\left(\frac{\partial p}{\partial t}\delta_{ij}-\frac{\partial \tau_{ij}}{\partial t}\right)+\frac{p\delta_{ij}-\tau_{ij}}{r^2}\right]dS \tag{4}$$

In this equation, 'r' represents the distance between the observer and the elementary sound source. One can note that the pressure fluctuation is evaluated from a volumetric and a surface integral. Therefore, a volumetric part of the mesh must be taken into account on the calculation of the propagation tool called “mcaa_waveprop” in CFD++/CAA++. It is important to verify that this part of the mesh must bound all the important fluid interactions and stress regions, no important turbulent activity can be outside the surface, under penalty of losing important information for the sound. These regions are pointed by Tam and Pastouchenko (2006), they suggest that the main noise source regions are: first, and one of the most important for the low frequencies, is the completely developed flow after the end of the potential core, another important source is the external shear layer for the higher frequencies followed by the inner shear layer which contributes for the same range of frequencies.

The noise was evaluated by a probe located at 90 degrees with the longitudinal direction of the jet at a radius of 64.5 D_s from the center of the jet exit plane as in the experimental data. At this location, the effects of reflection and refraction of the sound radiated can be neglected since this method do not take into account these effects.

2.3. Results and Discussion

This section presents the results of the set of simulations proposed, and some comparisons are made related to some previews computational works and experimental data.

The first sets of simulations that will be presented were carried out with the coplanar CoJeN nozzle showed on the Fig.1, and the results were compared to the previous work performed by Almeida (2009).

The results of Almeida (2009) were obtained with simulations using RANS based methodology together with a standard *k-ε* turbulence model within the *FLUENT*® solver applied to nozzles whose conditions and velocity ratios are employed in the present work. These comparisons are made with the aim to verify the methodology utilized here.

Secondly, a properly analysis of the influence of the velocity ratio is proceeded in order to obtain a clear understanding about what consequences it will bring to the far field noise results.

In the Figure 4 it is shown the center line velocity profile compared with the results by Almeida (2009), taking the results given by the simulation with area ratio AR = 3 and the velocity ratio VR = 1. It is expected that the behavior of the profile has some resemblance with that one given by a single jet in the same proportions.

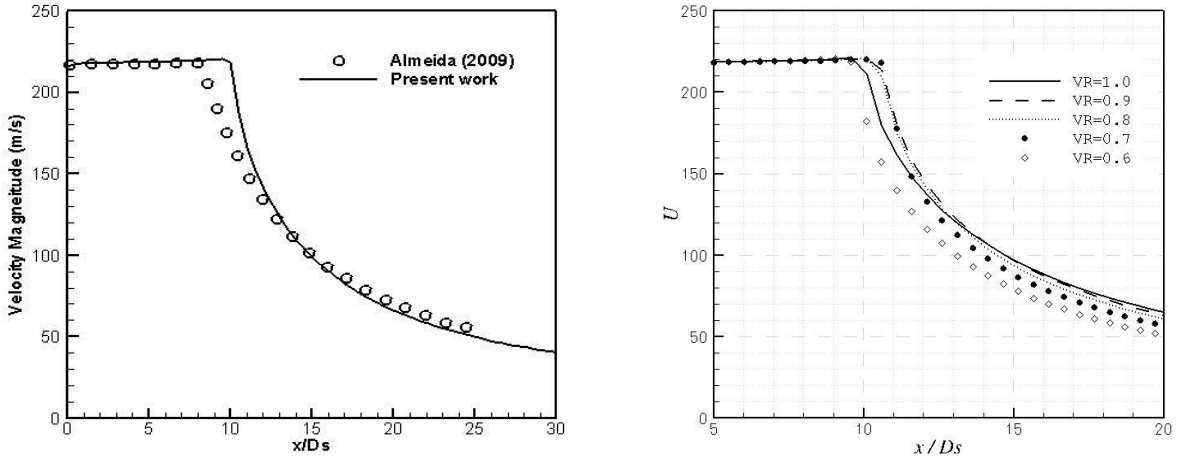

(a) (b)

Figure 4. Center line velocity profile for the coplanar nozzle. (a) A comparison between the VR=1.0 coplanar nozzle from Almeida (2009); (b) All the VR values of the present work.

According to the above figures the length of the potential core is over predicted, and this must be due to the turbulence model applied in this work which seems to give less dissipation on the interactions between the secondary and primary streams, and so the potential core is longer, reaching about 10 D_s. The error in predicting the length of the potential core implies on the displacement of the noise sources downstream on the jet. This is believed to be a consequence of the less effective mixing processes in the shear layer, which elongates the length of the potential core. Another probable cause is the turbulence level in the boundary condition of entry of the jet stream which are not possible to control. This over prediction can indicates that mixture process starts to happen later as indicated by Andersson et. al. (2005). Nevertheless, the velocity decay is quite in good agreement with the work of Almeida (2009), more precisely after the range x/Ds = [10;15] in which the velocity profile undergo a steeper decay.

The Figure 3(b) shows that the velocity decay is more pronounced for the smaller velocity ratios. When the secondary velocity is small, the energy of the potential core is rapidly extracted to the mixture process. On the same figure, an important behavior can be observed; the potential core length is slightly longer for the jet flow with velocity ratios VR = 0.7, 0.8 and 0.9, and smaller for the extreme values VR = 0.6 and 1.0. This is believed to be due to a combined influence of the both shear layers, the inner and the outer one.

It is noteworthy that, in this set of simulation (Table 1), the primary velocity remains constant while the secondary velocity is varied for the simulations. This situation modifies the velocity gradient on both shear layers which are the inner and outer. A higher secondary velocity (nearby the primary) leads to a weak shear effect on the inner shear layer, and a lower secondary velocity increases the stress on the inner shear layer and decreases it on the external one. This observation can be highlighted by verifying Figure 5, which presents the Turbulent Kinetic Energy (TKE) at different longitudinal positions (centerline and lipline) taken from the nozzle exit plane.

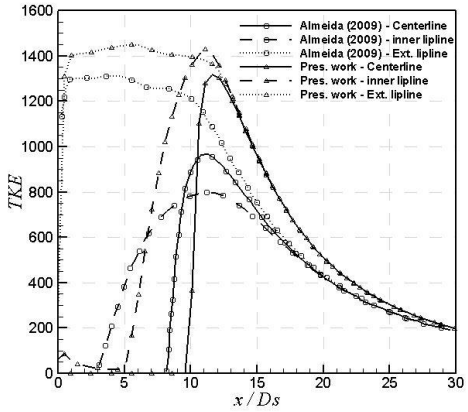

Figure 5. Center line and lip lines Turbulent Kinetic Energy profiles for the coplanar CoJeN nozzle with VR=1.0 in comparison to the work of Almeida (2009).

In the Figure 5, it is possible to see that the turbulence kinetic energy (TKE) profile was shifted about 2 D_s downstream, just like the end of the potential core. This effect of displacement can be seen on centerline with the position of peak, and also on the lip lines. The TKE peak on the simulation of the present work is higher than that presented in the work of Almeida (2009). This reaffirms the steep initial velocity decay from the end of the potential core presented in the Fig. 4(b).

Interesting is to notice that even with approximately values of velocity and the same geometry, the present work methodology leads to higher values of TKE energy. In other words, the velocity gradient on the outer shear layer is exactly the same in the two simulations in comparison but, nevertheless, the present profile of TKE is higher. This is believed to lead to a high value of peak of the inner lip line profile, and is certainly an effect due to the turbulence model.

First of all, the Fig. 6, as mentioned, shows how the turbulent kinetic energy behaves in the inner and the outer shear layers, as the secondary speed is modified. It is possible to identify that the centerline TKE profile do not change indicating that it is naturally just a consequence of the primary velocity.

Secondly, on the inner lip line profiles, the increasing of the secondary velocity influences tenuously just a few secondary diameters downstream of jet exit decreasing the TKE value. The external lip line in turn naturally have an increasing on the turbulent kinetic energy values starting with the region adjacent to the nozzle exit plane for the smaller secondary velocities and then all the profile along the potential core range gets a raise since about VR = 0.8. At this point, the outer shear layer starts to play an important role on the noise generation, being, in general, more important than the inner shear layer.

One can note that further downstream, the TKE profile reaches a greater value since the secondary velocity increases indicating a small spreading and slow velocity decay.

In that case, the turbulent kinetic energy peak is shifted and over predicted taking as base the work of Almeida (2009) suggesting that the turbulence model cubic k-ε is less dissipative than that one applied by the work which the author compared with.

These considerations must be analyzed with the thought of the over predicted potential core length, this is a good explanation for the displacement of the peak for example, since all the phenomena happens shifted in space, but this cannot explain the high values.

In the next figures, it is presented some comparisons among the different velocity ratios for coplanar configuration, the trend found matches with the behavior suggested by the literature. Despite, these results are supported by the curves of Length Scale and Time scale that have no significant change with the velocity ratio.

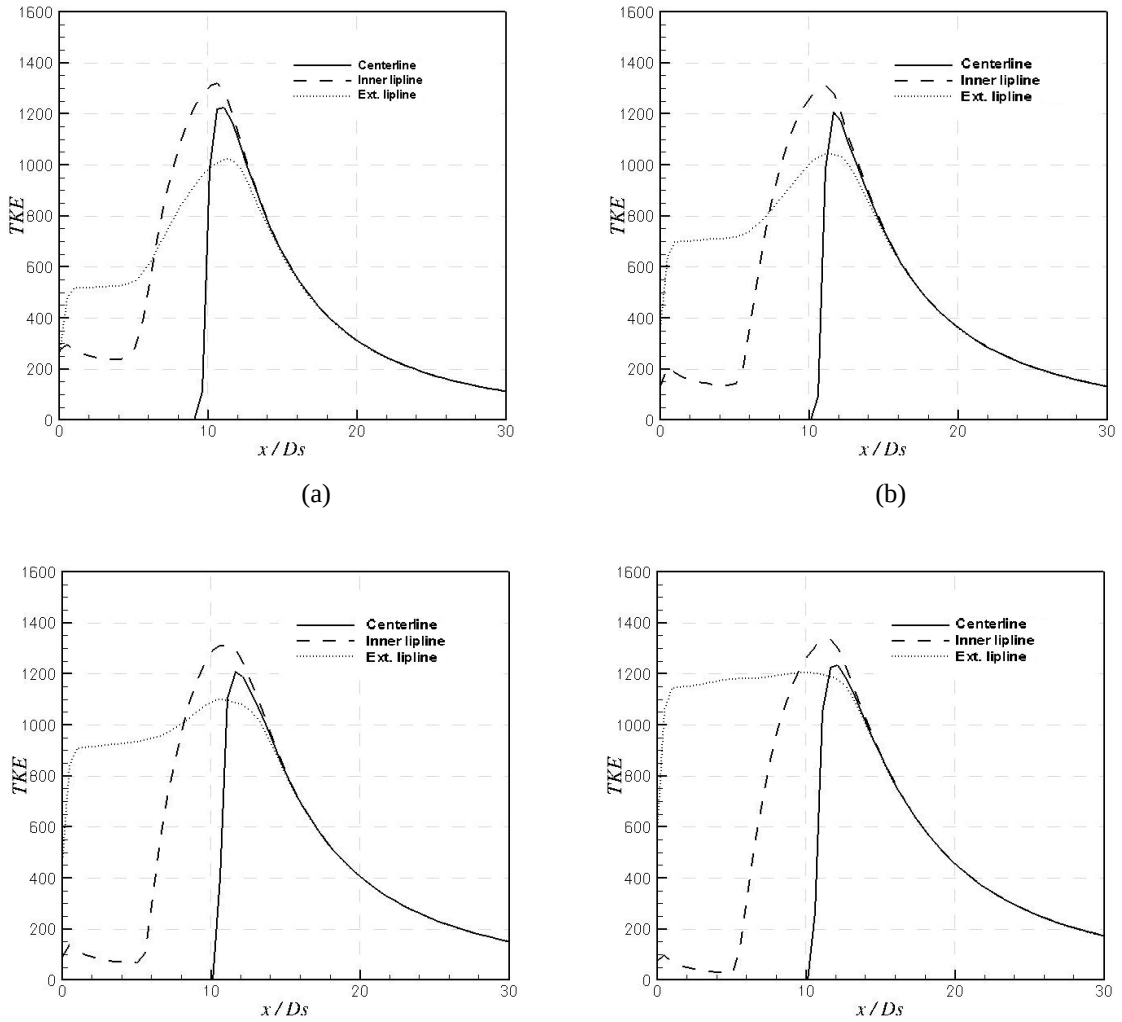

Figure 6. Turbulent Kinetic Energy for the remainder velocity ratio values to complement the Fig. 3. (a) VR=0.6; (b) VR=0.7; (c) VR=0.8; (d) VR=0.9.

The results about the area ratio AR = 2.0 for the JEAN configuration are presented below.

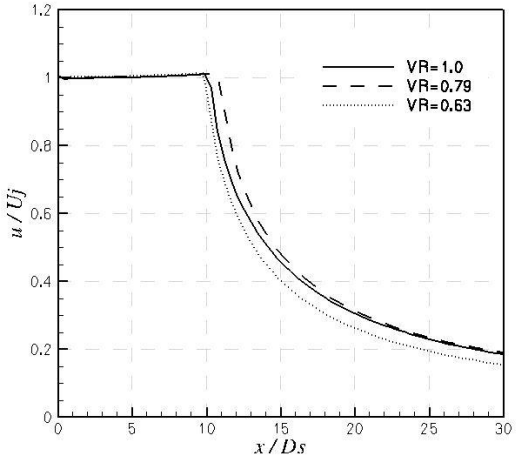

Figure 7. Centerline velocity profile comparison among the different velocity ratios for AR = 2.0.

Over again, the potential core length seems to be almost insensitive to the variation of exhaust velocities, and it seems to be weakly influenced by the area ratio when one compares the Fig. 7 and 9.

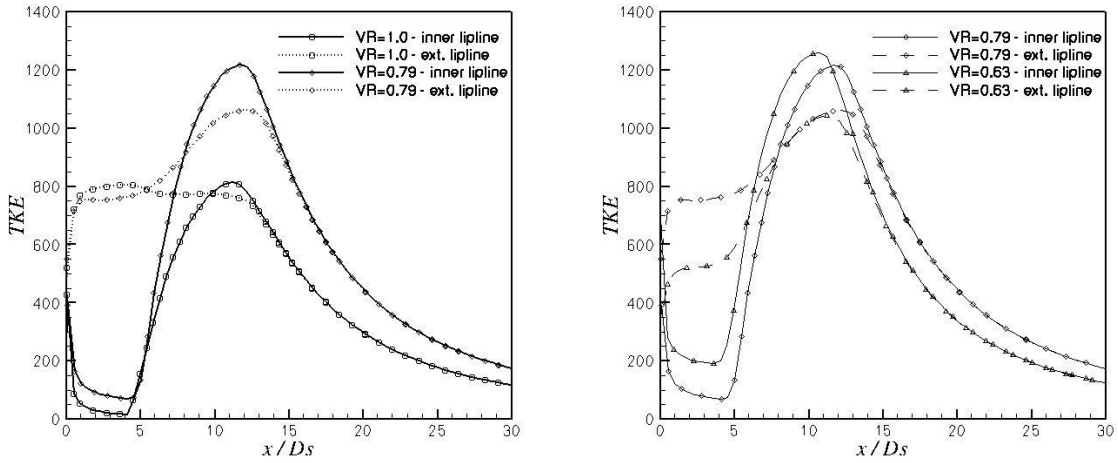

(a) (b)

Figure 8. Turbulent Kinetic Energy profiles for different velocity ratios. Comparison between: (a) VR=1.0 and VR=0.79; (b) VR=0.79 and VR=0.63.

The graphics in Fig. 8(a) and 8(b), compares two simulations with one parameter in common, the secondary and the primary velocity respectively. From the Figure 8(a), it is possible to conclude that the primary stream has no significant influence on the first region of the external shear layer, but it has, when the secondary potential core ends. This, on the graph is represented by the growth of the TKE on the external lip line.

In the Figure 8(b), one can see that for VR = 0.63, the influence of the primary stream on the external lip line profile starts early indicating that the potential core ends also early, this is related to the slightly smaller potential core length.

The results about the area ratio AR=4.0 JEAN configuration are presented below.

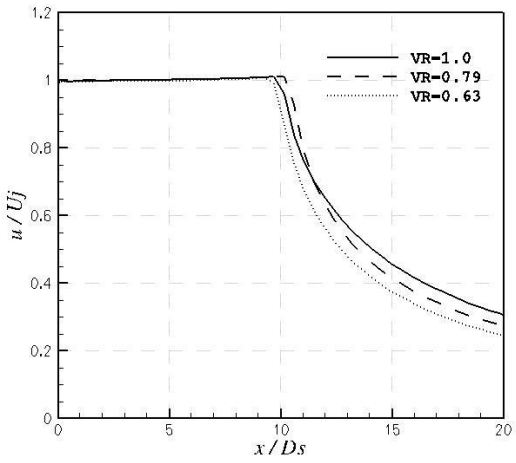

Figure 9. Centerline profile for the different velocity ratios for AR=4.0 on the JEAN geometry.

It can be noted that the behavior is quite similar to the other coplanar simulations with the velocity ratio changing. Here, again, the velocity decay is faster with the smaller velocity ratio values. The potential core length is softly changed with VR, but it does not seem to be directly proportional to this value, the behavior is a bit more complicated.

Here, the velocity decay is slower for VR = 1.0 than for VR = 0.79, and this is quite emphatic. This effect can be compared to the Fig. 7, where the difference on the rate decay seems to reduce, especially between VR = 1.0 and 0.79.

On the Figure 10(a), one can see that the primary stream, that before was contributing to increase the external lip line TKE values, here, for VR = 1.0, after the end of the secondary potential core, it is influencing for decrease it. This is believed to be causing the slightly smaller potential core length, in comparison with the median values of velocity ratio.

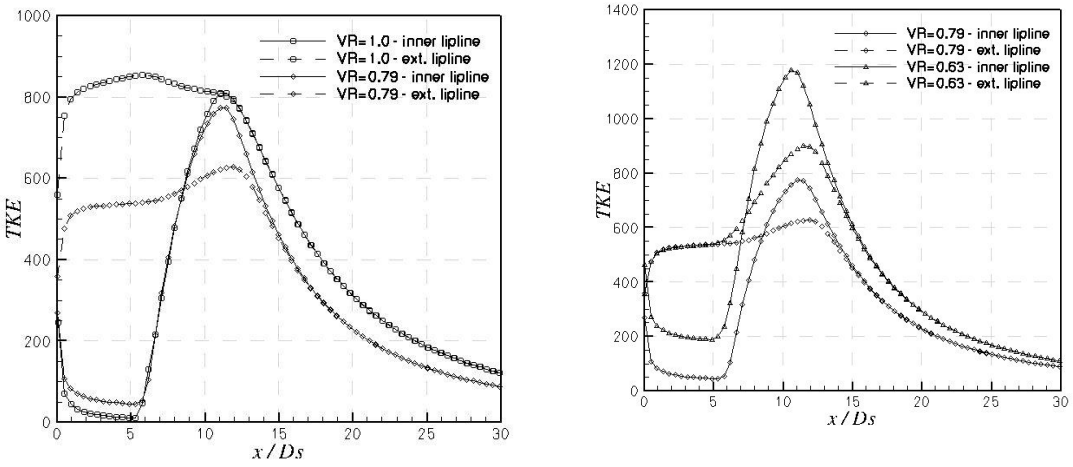

(a) (b)

Figure 10. Turbulent Kinetic Energy on the lip lines between: (a) VR=1.0 and VR=0.79; (b) VR=0.79 and VR=0.63.

The three-dimensional simulation presented below shows some differentiation on the properties, specially the turbulent kinetic energy which is directly influent on the noise generation, when comparing with the 2D values.

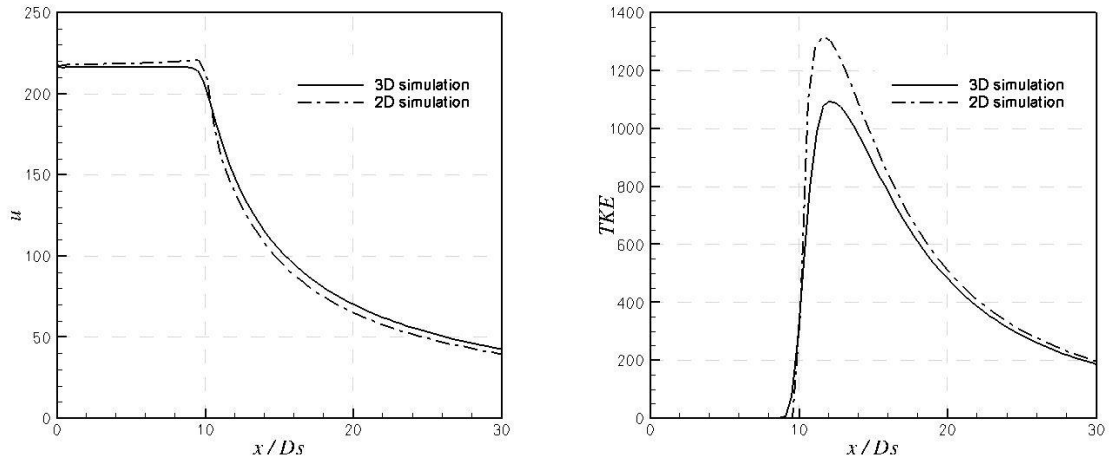

(a) (b)

Figure 11. Comparison between 2D and 3D centerline profiles.

The slight difference between the centerline velocity profile of 2D and 3D simulation certainly due to the lack of the three-dimensional effects of the turbulence on the first simulation, despites the residual of the latter one have been higher than the expected because of the convergence problems, possibly associated with the mesh generation.

This difference reflects on a quite large contrast on the peak of turbulent kinetic energy which can be seen on the Fig. 11(b). This difference is comparable to the difference between the turbulence kinetic energy peak given by the Almeida's (2009) solution and the present work's. Nevertheless comprehensively due to the lack of three-dimensional effects.

From now, it will be presented a preliminary acoustic result obtained by synthetic formulation discussed on section 2.2. Once the averaged fluid dynamic field was assessed from a three-dimensional mesh, the velocity fluctuation can be evaluated and the propagation model applied. For this, a virtual probe was positioned at 90 degrees normal to the jet at a distance of 64.5Ds in order to proceed the measuring of the pressure fluctuation. A fast Fourier transform is proceeded to the signal. The result can be seen in Fig. 12.

The sound pressure level found by the methodology was substantially below the experimental data at 30dB but the peak found at low frequencies and the shape of the profile are in agreement with the experimental data.

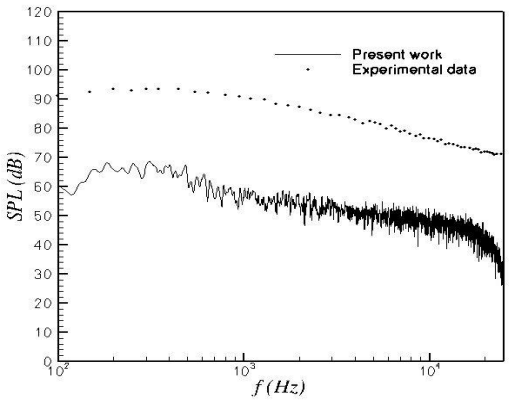

Figure 12. Comparison between the experimental noise result from the CoJeN project and the present simulation, for AR = 3.0 and VR = 1.0.

3. CONCLUDING REMARKS

The importance of understanding the phenomena involved in the coaxial jet flows was touched upon by the study presented from a practical perspective. Applying RANS methodology, it was pointed that, like was expected, the potential core was over predicted, but the developing of the spread and mixture process was quite in good agreement with the literature results. Thus, an initial understanding of the problem could be evaluated. Especially with regard to shear layers and the velocity and area ratios.

In consequence to the fluid dynamic results, the acoustic result is explainable under predicted but important information about the spectral profile and the peak of amplitude was in good agreement with the experimental data.

4. ACKNOWLEDGEMENTS

Thanks for Fluid Mechanics Laboratory (Mflab), Mechanical Engineering Faculty in the Federal University of Uberlandia and Aeronautic Industry (EMBRAER) for support with the CFD++/CAA++ software license.

5. REFERENCES

Almeida, Odenir de. 2009. Aeroacoustics of dual-stream Jets with Application to Turbofan Engines, São Paulo. Doctor thesis, Technological Institute of Aeronautics, São José dos Campos, SP, Brazil.

Andersson, N.; Eriksson, L. E.; Davidson, L. LES Prediction of Flow and Acoustic Field of a Coaxial Jet. 26th AIAA Aeroacoustics Conference, California, v.1, n.2884, pg. 1-26, 2005.

Birch, S. F; Lyubimov, D.A.; Secundov, A. N.; Yakubovsky, K. Ya. Numerical Modeling Requirements for Coaxial and Chevron Nozzle Flows. 9th AIAA/CEAS Aeroacoustics Conference and Exhibit, Hilton Head, South Carolina, v.1, n.3287, pg. 1-11, 2003.

Larsson, J. 2002. Computational Aero Acoustics for Vehicle Applications. Doctor thesis, Chalmers University of Technology, Göteborg, Sweden.

Silva, Carlos R. Ilário da, Almeida, O. de, Meneghini, Júlio R. Numerical and Empirical Approaches for Jet Noise Reduction: Investigation of Co-flow Effects. 30th AIAA Aeroacoustics Conference, Miami, FL, 2009.

Silva, Carlos R. Ilário da, Almeida, O. de, Batten, P. Invertigation of an Axi-symmetric Subsonic Turbulent Jet using Computational Aeroacoustics tools. 28th AIAA Aeroacoustics Conference, 2007.

Tam, C. K. W.; Pastouchenko, N. N. Fine-Scale Turbulence Noise from Dual-Stram Jets. AIAA Journal, v. 44, n. 1, pg. 90-101, 2006.

5. RESPONSIBILITY NOTICE

The authors are the only responsible for the printed material included in this paper.